Journal of Asian Ceramic Societies 1 (2013) 267–273

Contents lists available at ScienceDirect

Journal of Asian Ceramic Societies

journal homepage: www.elsevier.com/locate/jascer

TEM analysis of nanocrystalline SiC ceramics sintered by SPS using Al_2O_3–TiO_2 additive

Yutaka Shinoda [a,*], Yoshikazu Suzuki [b], Katsumi Yoshida [c]

[a] Secure Materials Center, Materials and Structures Laboratory, Tokyo Institute of Technology, Yokohama, Kanagawa 226-8503, Japan
[b] Faculty of Pure and Applied Science, University of Tsukuba, 1-1-1 Tennodai, Ibaraki 305-8573, Japan
[c] Research Laboratory for Nuclear Reactors, Tokyo Institute of Technology, 2-12-1 Ookayama, Meguro-ku, Tokyo 152-8550, Japan

ARTICLE INFO

Article history:
Received 2 May 2013
Received in revised form 17 June 2013
Accepted 25 June 2013
Available online 20 July 2013

Keywords:
Silicon carbide
Alumina
Titania
Spark plasma sintering
Mullite
TEM
EDS

ABSTRACT

Nanocrystalline SiC ceramics was fabricated by spark plasma sintering (SPS) using Al_2O_3 and TiO_2 additives with the composition of 5, 10 and 20 mass% (Al_2O_3–TiO_2). XRD analysis revealed formation of TiC phase. And also mullite phase with preferred orientation was detected in SiC with 20 mass% addition. From TEM observation and EDS analysis, TiC, aluminosilicate glass and mullite crystal phases were identified. Segregation of titanium atoms in addition to aluminum and oxygen atoms was observed at intergranular glassy phase with the thickness of 1–2 nm. The electrical conductivity was the same level as the Al_2O_3 single addition to SiC ceramics.

1. Introduction

Silicon carbide (SiC) ceramics exhibits excellent heat-resistance, creep-resistance, wear-resistance, acid-resistance and corrosion resistance properties and then could be applied as the structural components under extreme environments [1–5]. Covalent SiC powder compact is difficult to densify; therefore, the sintering additives, such as B–C co-doping, are usually used for its densification [6–10]. By using oxide additives that act at lower temperatures, it is also possible to decrease the sintering temperature and time. As for liquid-phase sintering of SiC ceramics, many kinds of systems mainly including alumina (Al_2O_3) have been investigated [11–13]. It is well known that the glassy phase is observed at grain boundaries or triple pockets in the liquid-phase sintered SiC ceramics. Such glassy phase degrades the mechanical properties of SiC such as hardness, creep resistance and high-temperature strength. In addition, the glassy phase affects the electrical conductivity while SiC ceramics is originally a semiconductor and exhibits relatively high electronic conductivity in the ceramic materials. Al_2O_3 addition to SiC ceramics has been reported to be effective to increase the electrical conductivity while beryllia (BeO) addition decreases it [14].

Similar covalent material, silicon nitride (Si_3N_4) ceramics, has superior strength and toughness properties at room temperature, and thus Si_3N_4 ceramics has been established itself as common structural ceramics. Generally, Si_3N_4 ceramics is densified by liquid-phase sintering using oxide additives. Hayashi et al. [15] reported that the wear resistance of Si_3N_4 ceramics was improved by the addition of small amount of titania (TiO_2). Using a detailed TEM observation, Yano et al. [16] revealed that the formation of titanium nitride (TiN) from TiO_2 improved the wear resistance of Si_3N_4 ceramics. Simultaneously, the formation of TiN phase by TiO_2 addition was reported to increase the electrical conductivity of Si_3N_4 ceramics by homogeneous distribution of TiN particles [17,18].

There are only a few reports of TiO_2 addition for sintering of SiC ceramics since TiO_2 itself does not contribute to densification of SiC ceramics [14]. Vlajic and Krstic [19] have made pressureless-sintered SiC with TiO_2 and Al_2O_3 additives. They reported that SiC was formed reacting with TiO_2 and TiC. SiC with 8 mass% TiO_2–7 mass% Al_2O_3 and with 4 mass% TiO_2–11 mass% Al_2O_3 exhibited maximum toughness and bending strength, respectively. Duan

* Corresponding author. Tel.: +81 45 924 5335; fax: +81 45 924 5339.
E-mail address: shinoda.y.ac@m.titech.ac.jp (Y. Shinoda).

Peer review under responsibility of The Ceramic Society of Japan and the Korean Ceramic Society.

Production and hosting by Elsevier

2187-0764 © 2013 The Ceramic Society of Japan and the Korean Ceramic Society. Production and hosting by Elsevier B.V. All rights reserved.
http://dx.doi.org/10.1016/j.jascer.2013.06.004

et al. [20] sintered amorphous silicon carbonitride (SiCN) powder with 20 mass% TiO_2 nanopowder by spark plasma sintering (SPS) and reported the formation of $TiC_{0.3}N_{0.7}$ particles resulting in improved fracture toughness, hardness and electrical conductivity.

In this way, the in situ TiC (or TiCN) dispersion in SiC using TiO_2 additive will be effective to improve the mechanical and electrical properties of SiC ceramics. Up to now, the local structure and the chemistry (i.e., grain boundaries or glassy pockets) in TiO_2 added SiC have not been well known. In this study, we fabricated the electrically conductive SiC ceramics with Al_2O_3–TiO_2 additive by spark plasma sintering (SPS) and investigated the microstructure in detail by transmission electron microscopy (TEM) observation and energy-dispersive X-ray spectrometry (EDS) analysis.

2. Experimental procedures

2.1. Sample preparation

The main starting powder was ultrafine β-SiC with a mean particle size of 60–80 nm (MTI Corp., Richmond, CA). By our measurement, the SiC powder actually contained 4.0 mass% impurity oxygen. The SiC powder was mixed with α-Al_2O_3 powder with a mean particle size of 0.2–0.3 μm (AKP-50; Sumitomo Chemical Co., Ltd., Tokyo, Japan) and TiO_2 powder with a mean particle size of 20 nm (MPT-881; Ishihara Sangyo Keisha, Ltd., Osaka, Japan) as sintering additives. The molar ratio of Al_2O_3 and TiO_2 powders was 1:1. The 5, 10 and 20 mass% (Al_2O_3–TiO_2) added SiC were named as 5, 10 and 20AT-SiC, respectively. The SiC and additive powders were planetary ball milled in pure ethanol using SiC pot and balls at 300 rpm for 1 h and dried in air at 80 °C. The mixed powders were sintered via SPS at 1800 °C at the pressure of 50 MPa, and the heating rate of 50 °C/min for 0–5 min under a nitrogen atmosphere. The electric current was shut down after soaking at 1800 °C.

2.2. Microstructural characterization

Crystalline phase identification of the samples was conducted by using X-ray diffractometry (XRD) (Rint 2500; Rigaku, Tokyo, Japan). TEM specimens were prepared by grinding to the thickness of <30 μm and by mirror polishing with 1 μm diamond paste before undergoing argon-ion milling at 5 keV using precision ion polishing system (PIPS, Model 691; Gatan Inc., Pleasanton, CA). TEM observation was performed with a field emission transmission electron microscope (FE-TEM, JEM2100F; JEOL Ltd., Tokyo, Japan) that was operated at 200 kV. The point-to-point resolution of this microscope was 1.9 Å. The grain boundaries were imaged edge-on. The analytical work was performed by energy-dispersive X-ray spectroscopy (EDS, JET2300T; JEOL Ltd., Tokyo, Japan) with the scanning transmission electron microscope (STEM) mode using a probe size of 1 nm.

2.3. Indentation testing

Indentation tests were conducted using a hardness tester (AVK-C2; Akashi Co., Ltd.). The samples were mirror polished and Vickers hardness and fracture toughness were measured under an indentation load of 19.6 N for 15 s.

2.4. Measurement of electrical conductivity

Electrical conductivity of the samples was measured by 4-Pin probe, constant-current method using a low resistivity meter (Loresta-EP; Mitsubishi Chemical Analytech Co., Ltd.).

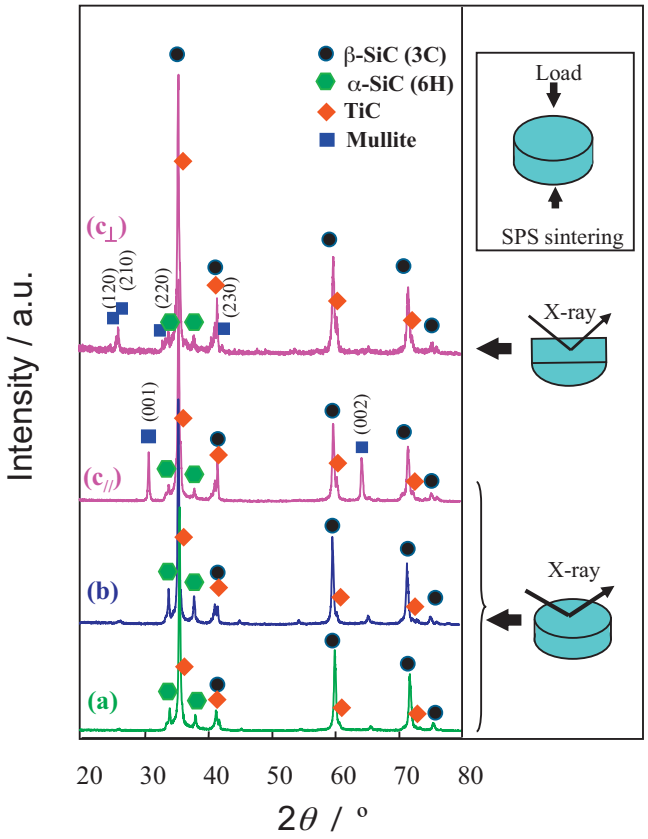

Fig. 1. XRD patterns of (a) 5AT-SiC, (b) 10AT-SiC and (c) 20AT-SiC.

3. Results and discussion

3.1. Constituent phases and microstructure

The bulk densities of sintered 5, 10 and 20AT-SiC measured by Archimedes method were 3.12, 3.11 and 3.17 g/cm^3, respectively. The densities corresponded to >97% of the theoretical density of SiC, i.e., 3.21 g/cm^3.

Fig. 1 shows XRD patterns of AT-SiC. The peaks from TiC were observed in all samples and the intensity of TiC peaks increased with increasing the amount of TiO_2 addition. The formation of TiC phase was considered to occur by following reaction:

$$SiC + TiO_2 \rightarrow TiC + SiO_2 \quad (1)$$

This reaction is thermodynamically favorable over a wide range of temperatures. The XRD results of 20AT-SiC were obviously different among the patterns from the parallel (Fig. 1($c_{\parallel}$)) and perpendicular (Fig. 1($c_{\perp}$)) planes to the compressive plane. The XRD pattern from the parallel plane ($c_{\parallel}$) included the peaks from (0 0 1) and (0 0 2) planes of mullite. On the other hand, the XRD pattern from the perpendicular plane ($c_{\perp}$) included the peaks from (1 2 0), (2 1 0), (2 2 0) and (2 3 0) planes of mullite, which are perpendicular to (0 0 1) plane of mullite. In this way, 20AT-SiC had the obvious oriented texture. The formation of mullite phase was explained by the following reaction:

$$(2+x)Al_2O_3 + 2(1-x)SiO_2 \rightarrow Al_{4+2x}Si_{2-2x}O_{10-x} \quad (2)$$

with x ranging between about 0.2 and 0.9 (corresponding to about 55–90 mol% Al_2O_3) [21]. Here assuming that most of the TiO_2 phase changed to TiC phase by reacting with SiC phase as the chemical equation (1); the total amount of SiO_2 phase in addition to the impurity silica in 20AT-SiC was ~14 mass%. In this case, the molar

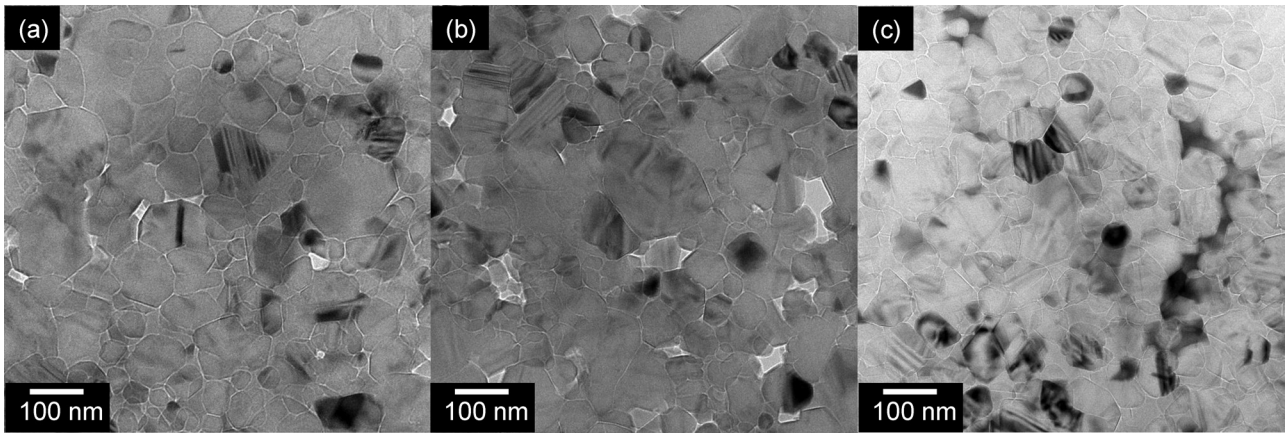

Fig. 2. TEM micrographs of (a) 5AT-SiC, (b) 10AT-SiC and (c) 20AT-SiC.

ratio of Al_2O_3 and SiO_2 is approximately 1:2 and then the excess SiO_2 was supposed to remain as the silica-rich glass.

Fig. 2 shows the TEM images of (a) 5AT-SiC, (b) 10AT-SiC and (c) 20AT-SiC. The incident direction of the electron beam was nearly perpendicular to the compressive plane of the each sample (in other words, the electron beam was almost parallel to the SPS compressive direction). Most of the grains were equi-axed nano grains with the size of ~100 nm. Some large grains with the size of ~300 nm were occasionally observed.

Fig. 3 presents a TEM micrograph and EDS spectra from (a) TiC grain and (b) SiC grain in 10AT-SiC. TiC grains usually have darker contrast than SiC matrix grains in TEM observation. The EDS spectrum confirmed that the darker grain substantially contained only Ti and C (Fig. 3(a)). Considering the XRD result, this grain can be identified as TiC grain. Assuming all of the added TiO_2 reacted with SiC grains and formed TiC grains, the volume fractions of the TiC phase of 5, 10 and 20AT-SiC were approximately estimated at 1, 2 and 4 vol.%, respectively. Glassy phase existed at multiple junctions of the grains. Si, Al and O atoms were confirmed at the multiple junctions in 10AT-SiC, suggesting the formation of aluminosilicate glass (Fig. 4). Assuming all of the added Al_2O_3 reacted with SiO_2 phase and formed mullite phase, its volume fractions were nearly 3.5, 7 and 14 vol.% for 5, 10 and 20AT-SiC, respectively. However, most of the added Al_2O_3 in 5 and 10AT-SiC was supposed to be contained in the aluminosilicate glass.

Fig. 5 shows the phase diagram of Al_2O_3–TiO_2–SiO_2 system [22]. We consider the sintering behavior of AT-SiC as follows. The compositions of initial state including impurity silica are marked by the cross symbol in the diagram. From this it is expected that the mullite phase would be formed during sintering. The solubility limits of TiO_2 in mullite are in ranges of 3.8–4.1 and 4.1–4.4 mass% TiO_2 for 3:2 mullite (i.e., $Al_6Si_2O_{13}$) and 2:1 mullite (i.e., Al_4SiO_8) series,

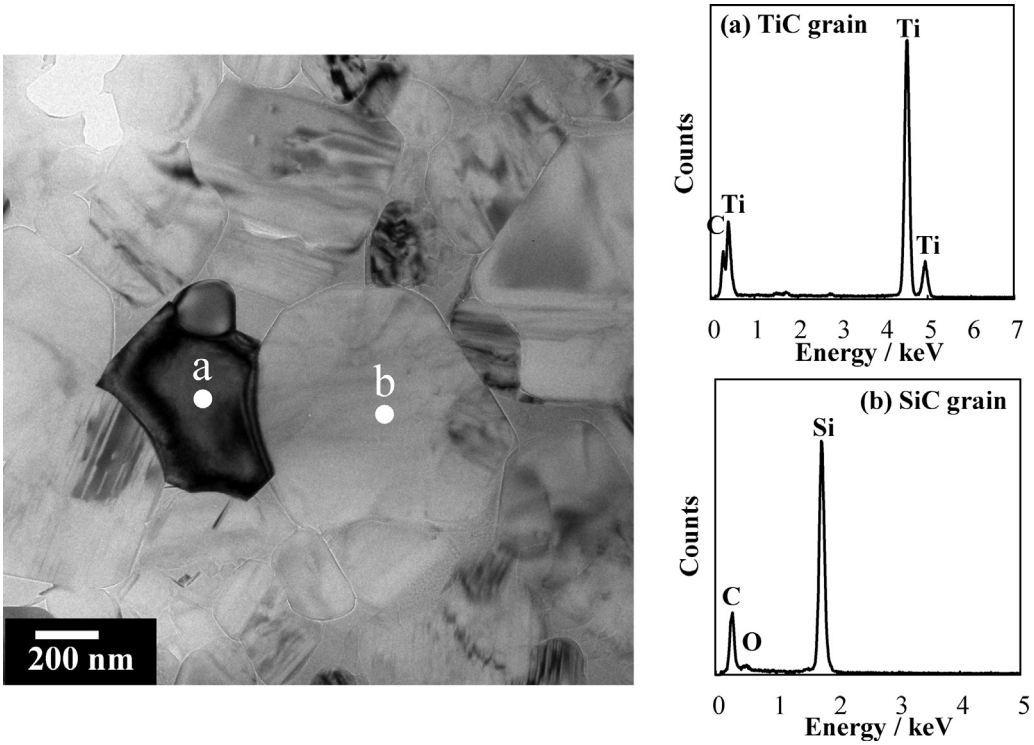

Fig. 3. TEM micrograph and EDS spectra from (a) TiC grain and (b) SiC grain in 10AT-SiC.

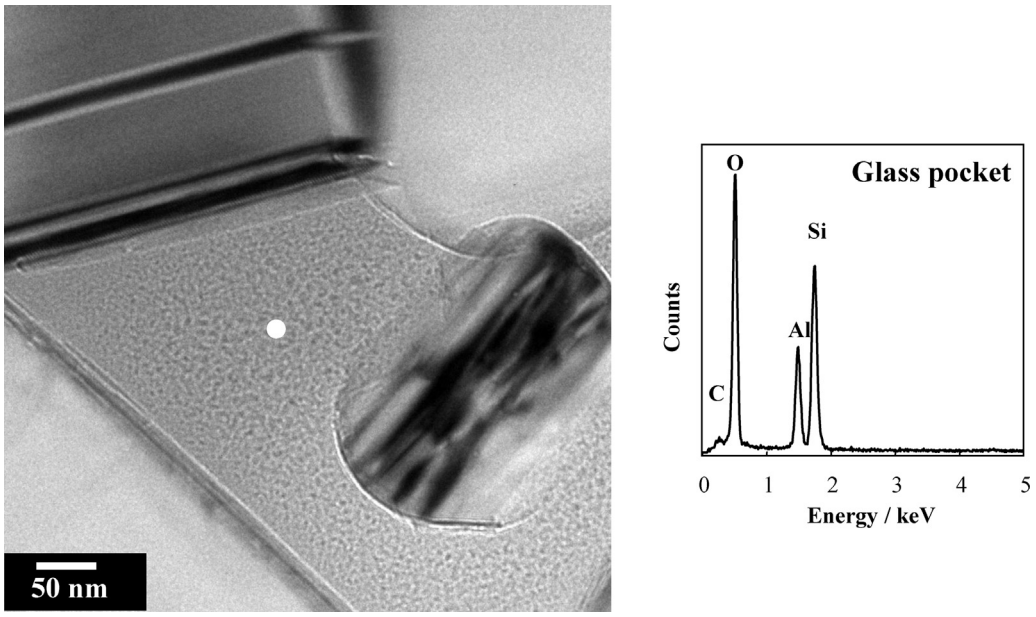

Fig. 4. TEM micrograph and EDS spectrum from glass pocket in 10AT-SiC.

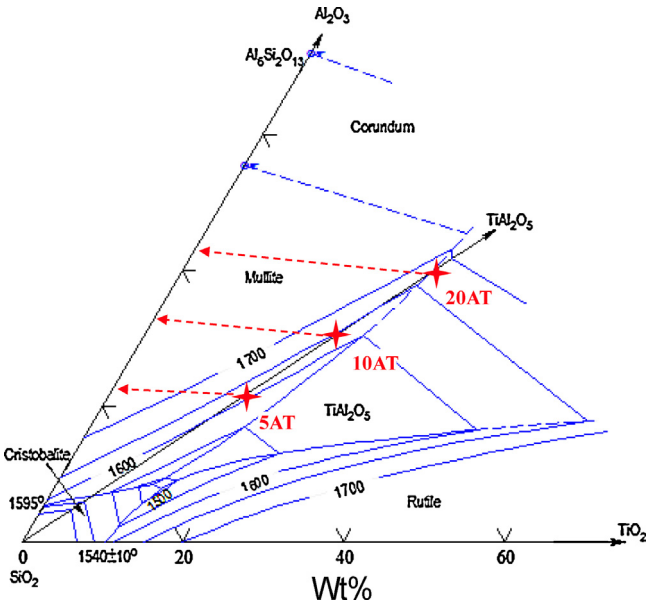

Fig. 5. Phase diagram of Al_2O_3–SiO_2–TiO_2 system [22]. The compositions of initial state including impurity silica are marked by the cross in the diagram.

respectively, at the temperatures between 1400 °C and 1600 °C [23]. The solubility limit of titanium atoms in SiC is 0.08 mass% at >2500 °C [24]. Thus the amorphous phase is thought to be aluminosilicate glass with TiO_2. However, during sintering TiO_2 phase reacted with SiC particles and then formed SiO_2 phase and TiC phase which was thermodynamically more stable than TiO_2 or $TiAl_2O_5$. Therefore, the titanium concentration in the glassy phase would decrease during sintering as denoted with arrows in the diagram. Finally the titanium atoms were rarely detected in the glassy phase.

Fig. 6 shows HRTEM micrographs of grain-boundary junction in 20AT-SiC. The initial stage nucleation of crystal phase from the glassy phase was observed (Fig. 6(a)). The SiC grains were surrounded by the crystallized pocket (Fig. 6(b)). The inset is Fast Fourier Transform (FFT) pattern at the pocket. The crystal phase in Fig. 6 is supposed to be mullite, as described below. HRTEM observation revealed that glassy phase (thickness of 1–2 nm), similar to that in Si_3N_4, existed at the SiC/SiC grain boundaries in 10AT-SiC (Fig. 7). The intergranular glassy phase was also observed in 5 and 20AT-SiC samples, and composed of Al, Si, O and C, which was confirmed by TEM-EDS analysis. It is worthy of note that Ti could not be detected in the glassy phase by the TEM-EDS analysis. The nondetection of Ti can be attributable to (1) insufficient resolution of TEM-EDS analysis or (2) intrinsic absence of Ti in the glassy phase. So, we performed STEM-EDS analysis with higher spatial resolution.

Fig. 8 presents STEM micrograph and EDS spectrum from mullite phase in 20AT-SiC. According to simplified determination, the ratio of the Al and Si atoms was 4:1. Therefore 2:1 mullite (i.e., Al_4SiO_8) was supposed to be formed at this region. The ratio of the Al and Si atoms changed depending on the measured points. The 2:1 mullite is commonly called as fused mullite and it is preferentially formed by crystallizing of aluminosilicate melt while the 3:2 mullite (i.e., $Al_6Si_2O_{13}$) is preferentially formed by solid-state reaction between Al_2O_3 and SiO_2 [25]. The sintering temperature (1800 °C) was lower than the melting temperature of mullite (~1850 °C); however, the real temperature of a sample during sintering by SPS has been reported higher than the measured temperature on the surface of graphite mold by a pyrometer [26,27]. So it was possible the mullite phase melted during sintering. Up to now the cause of the preferred orientation of mullite phase in 20AT-SiC is not clear, but it may relate to the formation process of mullite phase.

The STEM image and EDS spectra from (a) SiC/SiC grain boundary (G.B.), (b) glass pocket and (c) SiC grain in 20AT-SiC are presented in Fig. 9. The information from grain boundary with the thickness of ~1 nm shows the much higher amount of Al and O atoms existed at grain boundary than at SiC grain. The grain boundary is supposed to form the intergranular glassy phase as shown in Fig. 7. The peak at ~2.3 keV was caused by a molybdenum grid for supporting the TEM sample (MoLα: 2.293 keV). It should be noted that Ti atoms were detected at the grain boundary while they were not detected by TEM-EDS analysis. The amount of detection of Ti atoms was much smaller than those of Al or O atoms; however, Ti atoms could be surely considered to segregate at grain boundary by comparison with the spectra from SiC grain or glass pocket.

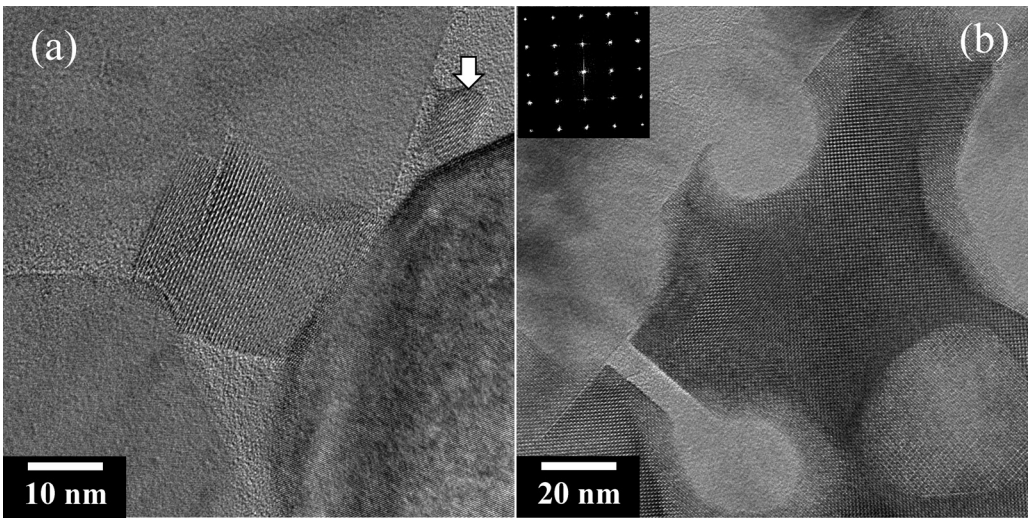

Fig. 6. HRTEM micrographs of crystal phase at grain-boundary junction in 20AT-SiC: (a) initial stage of nucleation (upper right), and (b) SiC grain was surrounded by mullite phase crystallized from liquid phase.

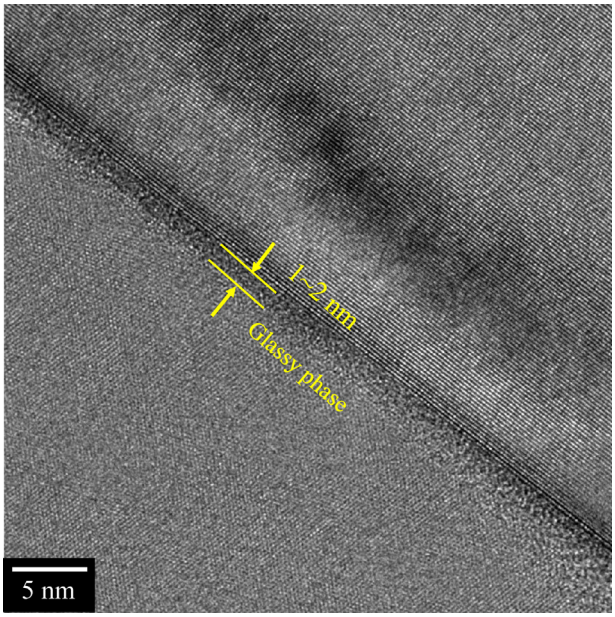

Fig. 7. HRTEM micrograph of intergranular glassy phase with the thickness of 1–2 nm in 10AT-SiC.

The TiO_2 phase was never observed alone and Ti atoms also were not detected in the silica or aluminosilicate glass and in the mullite phases. They almost reacted with SiC grains and form TiC grains. Thus, Ti atoms seem to more preferably combine with C atoms than O and Si atoms in the present system. So the intergranular segregated Ti atoms are expected to combine with C atoms on the outermost surface of SiC grain.

Table 1 summarized the results of the indentation tests. The fracture toughness of AT-SiC was calculated using Miyoshi's equation [28]. The fracture toughness of AT-SiC was not so high due to nano-grained microstructure. In particular, 5AT-SiC showed the low hardness and fracture toughness, because the secondary phase of 5AT-SiC was mainly composed of silica glass. The formation of TiC and mullite phase by co-doping of TiO_2 and Al_2O_3 was supposed to improve the mechanical property of SiC containing large amount of impurity silica owing to the formation of TiC and mullite phases. The control on the amount of additive and the grain size is expected to further improve the mechanical properties.

Table 1
Vickers hardness and fracture toughness of AT-SiC.

	Hardness, Hv	Fracture toughness, K_{IC} [MPa $m^{0.5}$]
AT5	1600 ± 80	2.2 ± 0.2
AT10	1980 ± 60	3.4 ± 0.2
AT20	1860 ± 30	3.6 ± 0.2

Loading, 19.6 N.

Fig. 10 shows electrical resistivity of AT-SiC using 4 Pin-probe, constant-current method. The data of 10 mass% Al_2O_3 doped SiC ceramics without TiO_2 addition (10A-SiC) and of boron and carbon doped SiC (B,C-SiC) are also included for comparison. The electrical resistivity of B,C-SiC was too high to measure by this method and it was over 10^6 Ω/□ that was measuring limit of the instrument. On the other hand, AT-SiC and 10A-SiC showed the much higher electrical conductivity than B,C-SiC. The electrical resistivities of AT-SiC and 10A-SiC were in the order of 10^2 Ω/□ which was lower by more than three order of magnitude than that of B,C-SiC. However, the dependence of the amount of Al_2O_3 addition besides the effect of TiO_2 addition was not remarkably observed. This meant that the electrical conductivities of them were dominated by a small amount of Al_2O_3 addition.

Al atoms diffuse into SiC grains during sintering and act as an accepter where they form the carriers, i.e. electron hole. The electrical resistivity of SiC is supposed to depend on the density of carrier in the SiC grains. The solubility limits of the Al atom at 1700 and 2200 °C are 1×10^{20} [29] and $7 \times 10^{20}/cm^3$ [30], respectively. Thus the solubility limit at present sintering temperature is presumed to be $\sim 10^{20}/cm^3$. The drastic reduction of electrical resistivity by addition of Al was possible to be caused by the solution of Al atoms in the SiC grains. On the other hand, Okano has reported that the electric current along grain-boundary phase was dominant on the electrical conduction of SiC sintered at <2000 °C because of the fine-grained microstructure, i.e. high volume fraction of grain-boundary phase, and that the highly concentrated additives and/or impurities at grain boundaries significantly increased the electrical conductivity [31]. Such effects on the electrical conductivity must depend on the kind of additives or impurities and on its combination. Therefore, a further detailed investigation is necessary to clarify them.

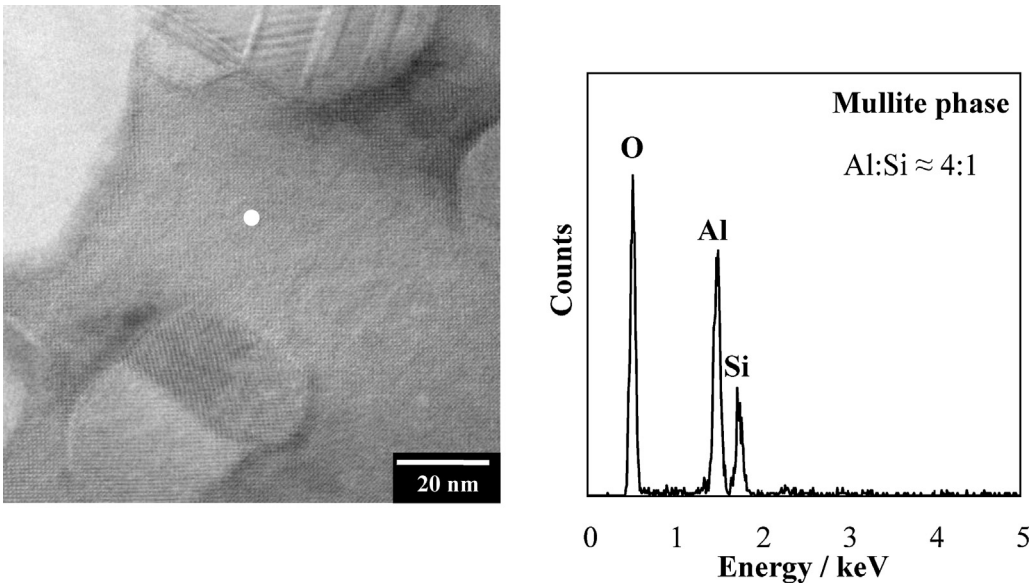

Fig. 8. STEM micrograph and EDS spectrum from mullite phase in 20AT-SiC.

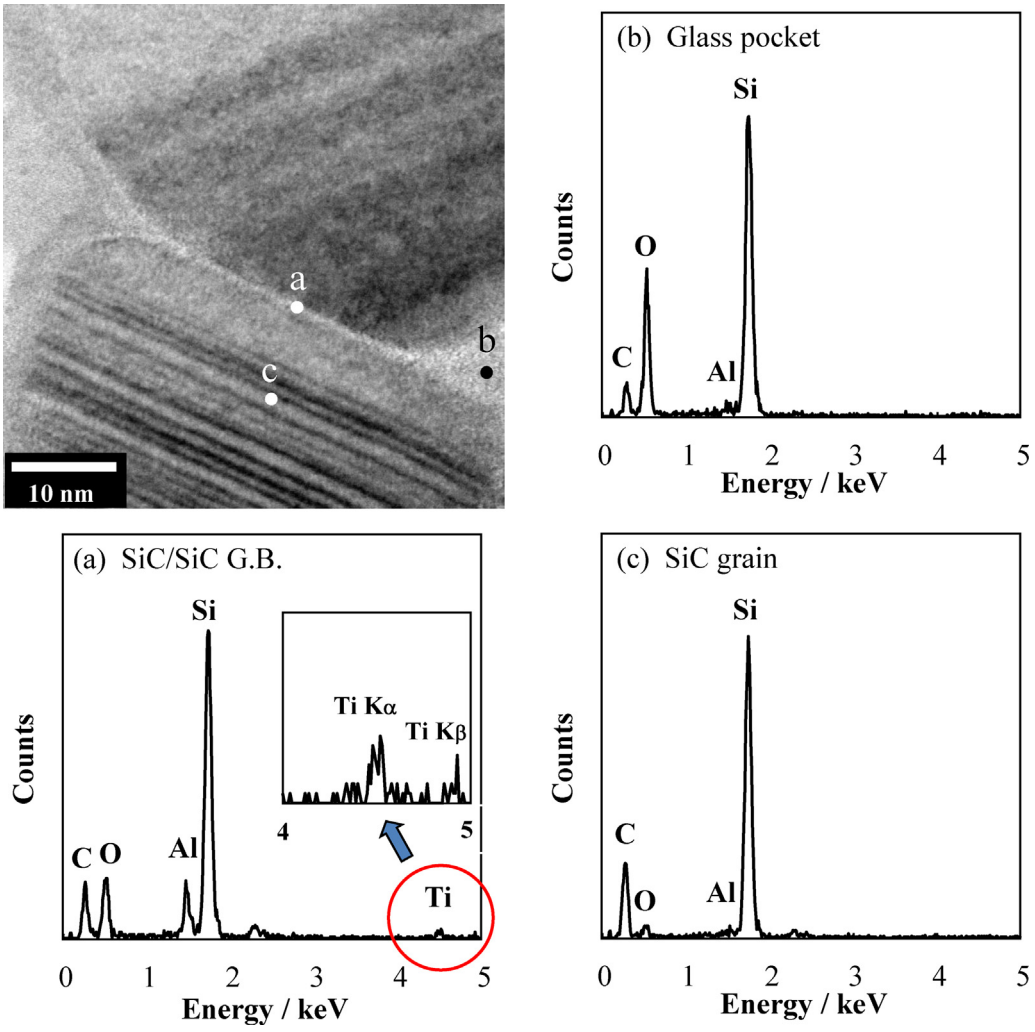

Fig. 9. STEM micrograph and EDS spectra from (a) SiC/SiC grain boundary (G.B.), (b) glass pocket and (c) SiC grain in 20AT-SiC.

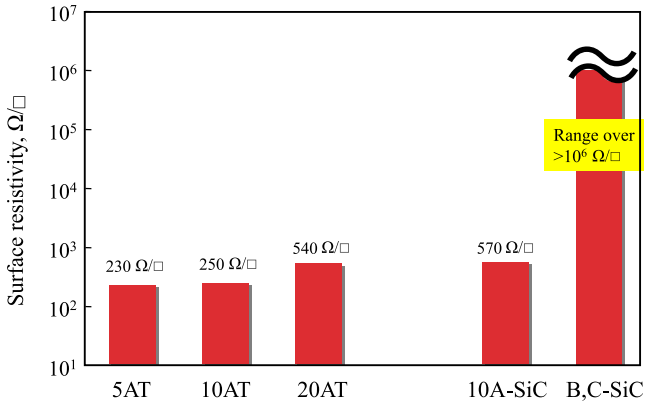

Fig. 10. Electrical resistivity of AT-SiC using 4 Pin-probe, constant-current method. The data of 10 mass% Al_2O_3 doped SiC (10A-SiC) and boron and carbon doped SiC (B,C-SiC) were presented as a comparison.

As above-mentioned, the volume fractions of the newly formed TiC phase of 5, 10 and 20AT-SiC were 1, 2 and 4 vol.% at the very most, respectively. Although TiC itself, indeed, was electrically conductive, such a small amount of formation of TiC phase was supposed to be not enough to increase the electrical conductivity of SiC considering the size and distribution of TiC grains.

In this study, we revealed the Ti atoms segregated at SiC/SiC grain boundaries in AT-SiC. However the amount of Ti segregation was very small and then its effect on electrical conductivity was restrictive in SiC doped with Al_2O_3. While the densification is not so easy, the influence of Ti single addition to SiC ceramics on the electrical conductivity is still of great interest because the added Ti atoms are possible to form the TiC-like local structure at the grain boundaries in SiC ceramics. The analysis using STEM-EELS (electron energy-loss spectroscopy) would be able to reveal the bonding state of Ti atoms at grain boundary.

4. Conclusion

Nanocrystalline SiC ceramics was prepared using Al_2O_3 and TiO_2 additives by SPS. TiC phase was formed by the reaction of TiO_2 additive and SiC grains in AT-SiC. Mullite phase with the texture where (0 0 1) plane of mullite was parallel to SPS compressive plane was detected by XRD analysis in 20AT-SiC. TEM observation identified the aluminosilicate glass and mullite crystal phase in AT-SiC. The glassy phase with thickness of 1–2 nm was observed at grain boundary in the AT-SiC. The intergranular glassy phase was mainly composed of Si, C, O and Al atoms. In addition, a small amount of Ti atoms were detected to segregate at grain boundaries by STEM-EDS analysis. The effect of TiO_2 addition to SiC ceramics doped with Al_2O_3 on surface resistivity was restrictive.

Acknowledgment

This work was supported by Collaborative Research Project of Materials and Structures Laboratory, Tokyo Institute of Technology.

Appendix A. Supplementary data

Supplementary data associated with this article can be found, in the online version, at doi:10.1016/j.jascer.2013.06.004.

References

[1] T. Narushima, T. Goto, T. Hirai and Y. Iguchi, Mater. Trans. JIM, 38, 821–835 (1997).
[2] K.S. Chan and R.A. Page, J. Am. Ceram. Soc., 76, 803–826 (1993).
[3] P.M. Sargent and M.F. Ashby, Scripta Metall., 17, 951–957 (1983).
[4] J.E. Lane, C.H. Carter and R.F. Davis, J. Am. Ceram. Soc., 71, 281–295 (1988).
[5] S.G. Cook, J.A. Little and J.E. King, Br. Corros. J., 29, 183–189 (1994).
[6] S. Prochazka, P. Popper, Special Ceramics, vol. 6, British Ceramic Research Association, Stoke-on-Trent, England, (1975) pp. 171–182.
[7] C. Greskovich and J.H. Rosolowski, J. Am. Ceram. Soc., 59, 336–343 (1976).
[8] T. Hase and H. Suzuki, J. Ceram. Soc. Jpn., 88, 258–264 (1980) [in Japanese].
[9] R.J. Hannink, Y. Bando, H. Tanaka and Y. Inomata, J. Mater. Sci., 23, 2093–2101 (1988).
[10] P. Elder and V.D. Krstic, Br. Ceram. Trans. J., 91, 67–71 (1992).
[11] M. Keppeler, H.G. Reichert, J.M. Broadley, G. Thurn, I. Wiedmann and F. Aldinger, J. Eur. Ceram. Soc., 18, 521–526 (1998).
[12] T. Nagano, H. Gu, K. Kaneko, G.D. Zhan and M. Mitomo, J. Am. Ceram. Soc., 84, 2045–2050 (2001).
[13] T. Nagano, K. Kaneko, G.D. Zhan, M. Mitomo and Y.W. Kim, J. Eur. Ceram. Soc., 22, 263–270 (2002).
[14] Y. Takeda, K. Nakamura, K. Maeda and Y. Matsushita, J. Ceram. Soc. Jpn., 95, 860–863 (1987) [in Japanese].
[15] T. Hayashi, J. Tatami, K. Komeya, T. Meguro and D.K. Kim, Proc. 19th Forum on Basic Science for High-Temperature Ceramics, (2000) pp. 25–27 [in Japanese].
[16] T. Yano, J. Tatami, K. Komeya and T. Meguro, J. Ceram. Soc. Jpn., 109, 396–400 (2001).
[17] S. Kawano, J. Takahashi and S. Shimada, J. Eur. Ceram. Soc., 24, 309–312 (2004).
[18] L. Gao, J. Li, T. Kusunose and K. Niihara, J. Eur. Ceram. Soc., 24, 381–386 (2004).
[19] M.D. Vlajic and V.D. Krstic, Solid State Phenomena, 25–26, 421–428 (1992).
[20] R.G. Duan, J.D. Kuntz, J.E. Garay and A.K. Mukherjee, Scr. Mater., 50, 1309–1313 (2004).
[21] R.X. Fischer, H. Schneider and D. Voll, J. Eur. Ceram. Soc., 16, 109–113 (1996).
[22] Y.M. Agamawi and J. White, Trans. Br. Ceram. Soc., 51, 293–325 (1952).
[23] R.S. Esther, J.S. Francisco, D.P. Estefanía, M.R. María, I.P. Ana, A.K. Marek, M.A. José and A. Javier, J. Eur. Ceram. Soc., 27, 2647–2654 (2007).
[24] G.L. Harris, Silicon Carbide, INSPEC (1995), pp. 153.
[25] H. Schneider, J. Schreuer and B. Hildmann, J. Eur. Ceram. Soc., 28, 329–344 (2008).
[26] D. Salamon, Z. Shen and P. Sajgalic, J. Eur. Ceram. Soc., 27, 2541–2547 (2007).
[27] J. Langer, D.V. Quach, J.R. Groza and O. Guillon, Int. J. Appl. Ceram. Technol., 8, 1459–1467 (2011).
[28] T. Miyoshi, N. Sagawa and T. Sassa, Jpn. Soc. Mech. Eng., 51, 2489–2497 (1985).
[29] M.K. Linnarsson, U. Zimmermann, J. Wong-Leung, A. Schöner, M.S. Janson, C. Jagadish and B.G. Svensson, Appl. Surf. Sci., 203–204, 427–432 (2003).
[30] Y. Tajima and W.D. Kingery, J. Am. Ceram. Soc., 65, C-27 (1982).
[31] K. Okano, J. Ceram. Soc. Jpn., 94, 219–225 (1986) [in Japanese].